ELSEVIER

Chemical Engineering Science 62 (2007) 4976–4982

Chemical Engineering Science

www.elsevier.com/locate/ces

Transient modeling of chemical vapor infiltration of methane using multi-step reaction and deposition models

Aijun Li, Olaf Deutschmann*

Institute for Chemical Technology and Polymer Chemistry, University of Karlsruhe, D-76131 Karlsruhe, Germany

Received 16 June 2006; received in revised form 25 January 2007; accepted 28 January 2007
Available online 17 February 2007

Abstract

Based on multi-step reaction and deposition models including the hydrogen inhibition model of pyrocarbon growth, transient 2D simulations of chemical vapor infiltration of methane were carried out by a finite element method (FEM) coupling the mass transfer (by convection and diffusion) and the evolutive surface area model with gas-phase and surface chemical reactions. The continuous infiltration, pyrolysis and deposition of methane and its consecutive C_xH_y products lead to continuously varying hydrogen concentration inside the carbon felt. The higher diffusibility of hydrogen compared to those of hydrocarbons results in complex distributions of $[H_2]/[C_xH_y]$ ratios inside the carbon felt, significantly affecting the deposition rates of pyrolytic carbon from hydrocarbons. The favorable densification mode (from inside to outside) seems to depend not only on the concentration ratio of $[C_2H_n]/[C_6H_m]$ but also on the concentration ratio of $[H_2]/[C_xH_y]$. The effect of various feed compositions of methane and hydrogen on densification of carbon felts was investigated at a temperature of 1368 K. An acceptable agreement was found between the predicted density distribution and experimental data taken from literature.

Keywords: C/C composites; Chemical processes; Materials processing; Mass transfer; Modeling; Porous media

1. Introduction

The chemical vapor infiltration (CVI), a chemical vapor deposition (CVD) in a porous substrate, is a promising process for the production of continuous fiber reinforced ceramic composites such as carbon/carbon (C/C) composites (Besmann et al., 1991; Fitzer, 1987). In carbon CVI, gaseous or liquid precursors diffuse or are forced into a heated fiber preform placed in a reactor the details of which are described elsewhere (Benzinger and Hüttinger, 1998; Hu and Hüttinger, 2001; Vignoles et al., 2006). In the porous structure, the precursor undergoes a complex chemical reaction network, eventually forming solid matrix deposits on the surface of the fibers. As a contrast to CVD, the interaction of homogeneous gas-phase and heterogeneous surface reactions involved in CVI are dramatically enhanced due to the large and dynamic bulk surface formed by numerous and circumferential-growing fibers. Therefore, the development of detailed chemical reaction mechanisms for CVI for a long time has been a scientific goal in order to improve the production of C/C, in particular to optimize microstructures leading to the desired physical and mechanical properties of the synthesized materials. CVD of pyrolytic carbon from light hydrocarbons such as methane, ethylene, acetylene and benzene has been investigated recently. Widely accepted results of those studies are (1) gas-phase reactions produce hydrocarbon species with increasing number of carbon atoms; (2) hydrocarbons with increasing size show increasing deposition rates, but the hydrogen inhibition of carbon deposition from the hydrocarbon also increases due to different molecular structures; (3) the dissociation of carbon–hydrogen surface complexes should be the rate-controlling step of carbon deposition (Delhaès, 2002; Becker et al., 2000). These findings provided a guideline on modeling the CVI process.

Many models have been proposed to simulate the growth of a matrix on fibers based on only an overall reaction (Starr, 1988; Tai and Chou, 1989; Sheldon and Besmann, 1991). These models paid much attention to modeling of physical properties such as the surface area per volume, the gas permeability and

* Corresponding author. Tel.: +49 721 608 3064; fax: +49 721 608 4805.
E-mail addresses: li@ict.uni-karlsruhe.de (A. Li), deutschmann@ict.uni-karlsruhe.de (O. Deutschmann).

0009-2509/$ - see front matter © 2007 Elsevier Ltd. All rights reserved.
doi:10.1016/j.ces.2007.01.069

mass/heat transfer. Therefore, from the viewpoint of chemical reactions, these models are not sufficiently instructive to reveal the essentials of CVI processes. During the past decade, several reduced chemical reaction mechanisms have been developed to simulate pyrolytic carbon deposition (see e.g. Birakayala and Evans, 2002). In these models, various reaction pathways from light species to aromatic species were proposed, leading to a deeper insight into the chemistry of C/C CVI. However, only the initial stage of the CVI processes or 1D simulations were considered in their works. Based on the multi-step reaction and deposition model, taking into account the inhibiting effect of hydrogen on carbon deposition (the hydrogen inhibition model), transient 2D simulations of CVI for the densification of carbon fiber felts with pure methane or mixtures of methane and hydrogen as feed gases were performed in the present work. All necessary gas-phase kinetic data were calculated using a reduced mechanism and surface reaction kinetic data were derived from the results of CVD experiments (Becker and Hüttinger, 1998a, b). Simulated densification results of carbon fiber felts were compared with experimental data.

2. Modeling approach and numerical simulation

Generally, the chemistry in the homogeneous gas phase leads to the formation of aliphatic compounds, ethylene and acetylene, and, for the aromatic route, benzene-type species and the formation of PAHs, while heterogeneous surface chemistry results in variously textured pyrolytic carbons from different gaseous organic compounds in CVD processes. The most widely accepted empirical model of the complex surface reaction network involved in CVD was proposed by Hüttinger (1998), in which a consecutive reaction path was assumed. From the viewpoint of simulation, this model has the advantage that all surface reaction kinetic data corresponding to zero residence time can be measured and calculated directly by CVD experiments. These kinetic data, however, seem to be unsuitable for modeling CVI processes. The most important reason is that the amounts of hydrogen formed by continuous infiltration, pyrolysis and deposition of hydrocarbons during CVI significantly exceed those formed during CVD processes. The resultant hydrogen limits the deposition rates of carbon from hydrocarbons, due to an inhibition of reactions at the carbon surface because hydrogen forms very stable carbon–hydrogen surface complexes ($\Delta E_{C-H} \approx 480\,\mathrm{kJ\,mol^{-1}}$) at the edge atoms of the graphene layers. In the present paper, the multi-step homogeneous reaction model was coupled with the heterogeneous surface reaction model of hydrogen inhibition on pyrocarbon deposition, as shown in Fig. 1. All gas-phase kinetic data, k_1–k_4 ($\mathrm{s^{-1}}$), were taken from the multi-step "parallel-consecutive" model (Li et al., 2005). The concentrations ($\mathrm{mol\,m^{-3}}$) of methane, ethylene, acetylene, benzene and hydrogen were defined as c_i ($i = 1, 2, \ldots, 5$).

Surface reaction kinetic data, k_5–k_8 ($\mathrm{m\,s^{-1}}$), were derived from the hydrogen inhibition model originally proposed by Becker et al. (2000). As a model reaction, the following shows carbon deposition from acetylene, including an irreversible chemisorption of a hydrocarbon species at a free active site

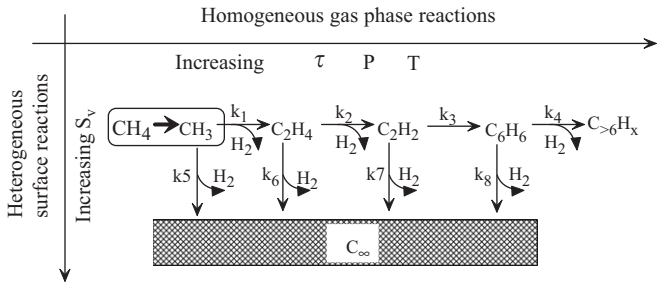

Fig. 1. A multi-step deposition model with consideration of the hydrogen inhibition.

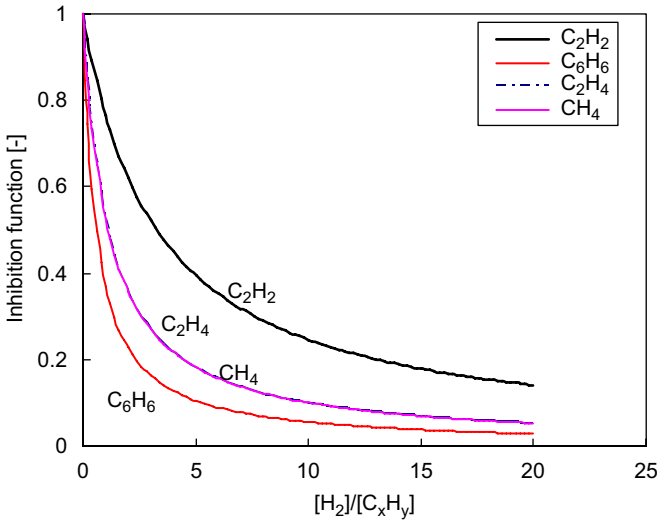

Fig. 2. Inhibition functions of various hydrocarbons (profile of CH_4 at 1373 K, others at 1273 K) as a function of the hydrogen content.

(Eq. (1)) and a reversible desorption of hydrogen (Eq. (2)):

$$C_\infty() + C_2H_2 \xrightarrow{k_1} C_\infty(H_2), \tag{1}$$

$$C_\infty(H_2) \underset{k_{-2}}{\overset{k_2}{\rightleftharpoons}} C_\infty() + H_2, \tag{2}$$

where $C_\infty()$ defines a free surface active site and $C_\infty(H_2)$ an active site blocked by chemisorbed hydrocarbon. The total number of surface sites, c, is the sum of both free surface active sites and blocked surface sites,

$$c = c_\infty() + c_\infty(H_2). \tag{3}$$

The rates of reactions (1) and (2) can be defined as follows:

$$r_1 = k_1 \cdot c_\infty() \cdot P_{C_2H_2}, \tag{4}$$

$$r_2 = k_2 \cdot c_\infty(H_2) - k_{-2} \cdot c_\infty() \cdot P_{H_2}. \tag{5}$$

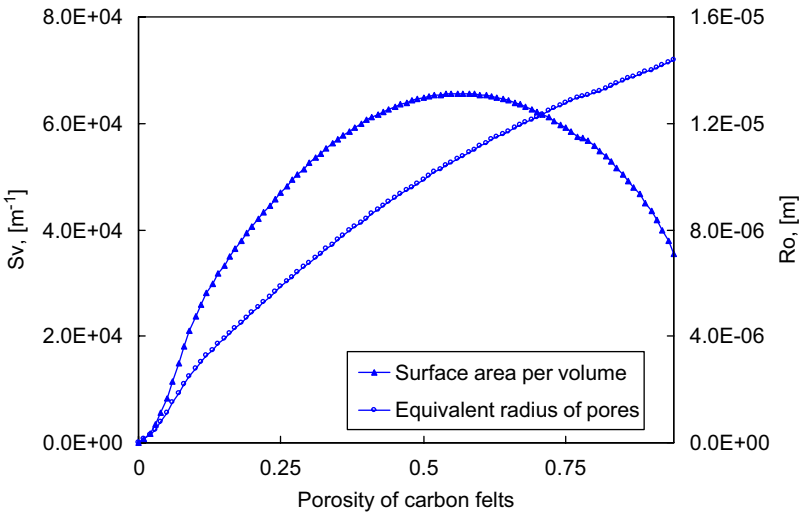

Fig. 3. Evolutions of the surface area per volume and the equivalent radius of pores of carbon felts.

At steady-state conditions, the rates of reactions (1), (2) and the rate of carbon deposition at the surface carbon r_s (mol m^{-2}) are equal:

$$r_s = r_1 = r_2. \tag{6}$$

Combining Eqs. (3)–(6) leads to:

$$\begin{aligned} r_s &= \frac{c \cdot k_1 \cdot P_{C_2H_2}}{1 + \dfrac{k_{-2}}{k_2} P_{H_2} + \dfrac{k_1}{k_2} P_{C_2H_2}} \\ &= \frac{c \cdot k_1}{\dfrac{1}{P_{C_2H_2}} + \dfrac{k_{-2} \cdot P_{H_2}}{k_2 \cdot P_{C_2H_2}} + \dfrac{k_1}{k_2}} \\ &= \frac{c \cdot k_1 \cdot \dfrac{k_2}{k_{-2}}}{\dfrac{k_2}{k_{-2} \cdot P_{C_2H_2}} + \dfrac{k_1}{k_{-2}} + \dfrac{P_{H_2}}{P_{C_2H_2}}}. \end{aligned} \tag{7}$$

Due to the high stability of carbon–hydrogen surface complexes, $k_2 \ll k_{-2} P_{C_2H_2}$ and then $k_2/k_{-2} P_{C_2H_2} \approx 0$. By introducing the ideal gas law into Eq. (7), one obtains

$$r_s \approx c \cdot k_2 \cdot \frac{\dfrac{k_1}{k_{-2}}}{\dfrac{k_1}{k_{-2}} + \dfrac{c_5}{c_3}}. \tag{8}$$

As defined above, c_3 and c_5 are concentrations of acetylene and hydrogen, respectively. Then the rate constant of carbon deposition from acetylene per unit surface area as shown in Fig. 1, k_7 (m s^{-1}), can be calculated from:

$$k_7 = \frac{r_s}{c_3} \approx \left(\frac{c \cdot k_2}{c_3}\right) \cdot \left(\frac{\dfrac{k_1}{k_{-2}}}{\dfrac{k_1}{k_{-2}} + \dfrac{c_5}{c_3}}\right). \tag{9}$$

The first part of the above formula can be defined as the original deposition rate constant per unit surface area, the second part as the hydrogen inhibition coefficient, shown below:

$$k_7' = \frac{c \cdot k_2}{c_3}, \tag{10}$$

$$I_{C_2H_2} = \frac{\dfrac{k_1}{k_{-2}}}{\dfrac{k_1}{k_{-2}} + \dfrac{c_5}{c_3}}. \tag{11}$$

For the residence time zero, the original deposition rate constants of gas-phase species were calculated by CVD-experiments (Brüggert et al., 1999; Becker and Hüttinger, 1998a, b). Moreover, the hydrogen inhibition functions for these species were also derived (shown in Fig. 2), based on experimental data of Becker et al. (2000). Since there were not enough experimental data up to now, only hydrogen inhibition functions at given temperatures are presented in this paper. The formula of the hydrogen inhibition functions are given by Eqs. (12) and (13):

$$I_{CH_4} = \frac{1.112}{1.112 + \dfrac{c_5}{c_1}}, \quad I_{C_2H_4} = \frac{1.104}{1.104 + \dfrac{c_5}{c_2}}, \tag{12}$$

$$I_{C_2H_2} = \frac{3.269}{3.269 + \dfrac{c_5}{c_3}}, \quad I_{C_6H_6} = \frac{0.589}{0.589 + \dfrac{c_5}{c_4}}. \tag{13}$$

The principle difference between CVI and CVD is the large surface area dynamically increasing with progressive densification of porous substrates. In the present work, a porosity model of carbon felts with randomly distributed, non-overlapping fibers was generated and then the evolution of surface area per volume, S_v (m^{-1}), was calculated numerically. Fig. 3 shows S_v profiles of carbon felts with various initial fiber volume fractions.

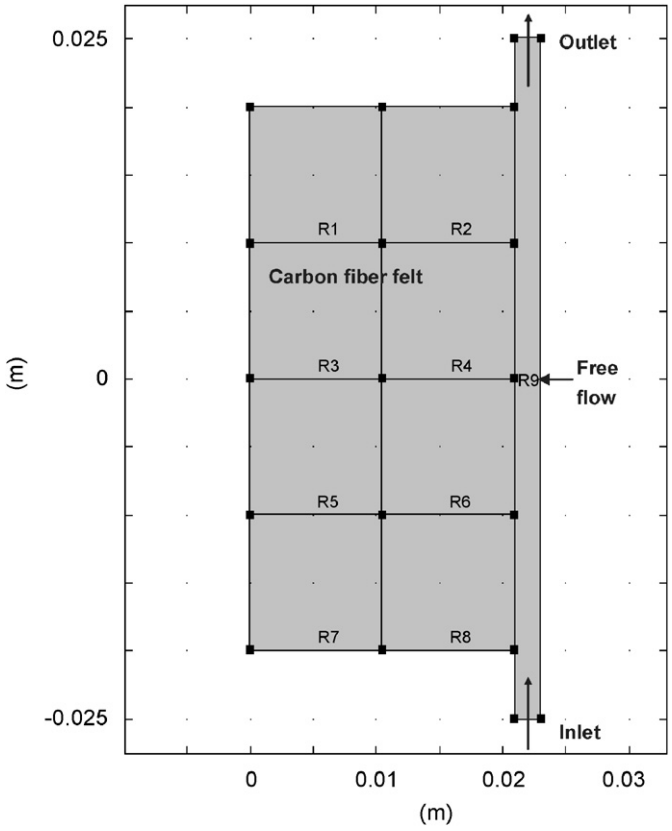

Fig. 4. The simplified 2D symmetrical geometry; subdomains R1–R8 represent the carbon fiber felt and subdomain R9 represents the free flow space of the CVI reactor.

Based on the above models, 2D transient mass transfer equations of hydrocarbons and hydrogen as well as the porosity equation are employed as follows:

$$\begin{cases} \dfrac{\partial c_i}{\partial t} + \nabla \cdot (-D_i \nabla c_i + c_i \mathrm{U}) = R^i_{(c_1,c_2,c_3,c_4,c_5)}, & i = 1,2,\ldots,5 \text{ in free flow space,} \\ \dfrac{\partial c_i}{\partial t} + \nabla \cdot (-D_i^{\mathrm{eff}} \nabla c_i) = R^i_{(S_v,c_1,c_2,c_3,c_4,c_5)}, & i = 1,2,\ldots,5 \text{ inside felt,} \\ \dfrac{\partial e}{\partial t} = -\dfrac{M_C}{\rho_C} R^C_{(S_v,c_1,c_2,c_3,c_4,c_5)} & \text{inside felt,} \\ \dfrac{\partial \rho}{\partial t} = M_C R^C_{(S_v,c_1,c_2,c_3,c_4,c_5)} & \text{inside felt.} \end{cases} \quad (14)$$

Here, D_i and D_i^{eff} ($\mathrm{m^2\,s^{-1}}$) are the diffusion coefficients in the free flow space and the effective ones in the porous medium, respectively. The latter depends on the tortuosity factor and the equivalent radius of pores of the porous medium. U ($\mathrm{m\,s^{-1}}$) is the flow velocity in the narrow gap (the free flow space shown in Fig. 4). This convective flow can be modeled as a plug flow or a fully developed laminar flow without having an impact on CVI simulation results. R^i ($\mathrm{mol\,m^{-3}\,s^{-1}}$) represents the chemical source terms in two different subdomains. e and ρ ($\mathrm{kg\,m^{-3}}$) denote the porosity and bulk density of the substrate, respectively. M_C ($\mathrm{kg\,mol^{-1}}$) is the molar mass of carbon; ρ_C ($\mathrm{kg\,m^{-3}}$) is the density of pyrolytic carbon, which is not constant, because it corresponds to the varying texture of the pyrolytic carbon formed on fiber surface (Delhaès, 2002). However, an average density of pyrolytic carbon is assumed in the present work. The subdomain setup of the reactor geometry is presented in Fig. 4. The finite element method (FEM) platform, COMSOL Multiphysics, was applied for our transient 2D simulations of CVI processes.

3. Results and discussion

The hydrogen inhibition for carbon deposition was investigated by simulations of three sets of experiments corresponding to feed gases of 20 kPa pure CH_4, 20 kPa CH_4 with additional 4 kPa H_2 and 20 kPa CH_4 with additional 10 kPa H_2, respectively. All experiments were carried out at a temperature of 1368 K, an infiltration time of 120 h, an initial fiber volume fraction of 7.1% and a residence time of 0.1 s (Zhang and Hüttinger, 2002).

The result of the simulation for the CVI experiment using pure methane as precursor is presented in Fig. 5(a). The density slightly decreases from the outside to the inside of the felt, which indicates the inception of a diffusion limitation. Figs. 5(b) and (c) show the predicted density distributions for the CVI experiments using methane with additional hydrogen of 4 and 10 kPa H_2 as the feed gas, respectively. The inside–outside densification mode achieved in Figs. 5(b) and (c) reveals that additional hydrogen is helpful to avoid premature surface crusting. In fact, the inside–outside densification mode is achieved in the first 60 h of densification for all three cases. Fig. 6 shows the predicted bulk density distributions of the three cases corresponding to 60 h of densification. Higher out-diffusibility of hydrogen can automatically result in a lower densification rate near the surface of the felt, which slightly favours a reaction-controlled overall process. The amount of hydrogen generated by gas-phase and surface reactions, however, is not enough to ensure this favorable shift throughout the 120 h densification. Comparing Fig. 5 with Fig. 6 one can recognize that, additional hydrogen obviously is very beneficial to both an inside–outside densification mode and a homogeneous densification from the bottom to the top of carbon felts, though it will decrease the total deposition rate.

Simulation results for pure methane and methane plus 4 kPa H_2 agree with experimental results published by Zhang and Hüttinger (2002), as shown in Figs. 7(a) and (b). However, it is obvious that too much additional hydrogen will result in not only a slow deposition but also in a dramatic debasement of the pyrocarbon textures, indicated by very low bulk densities, to be recognized in both Fig. 5(c) to (a) and Fig. 6(c) to (a). In the

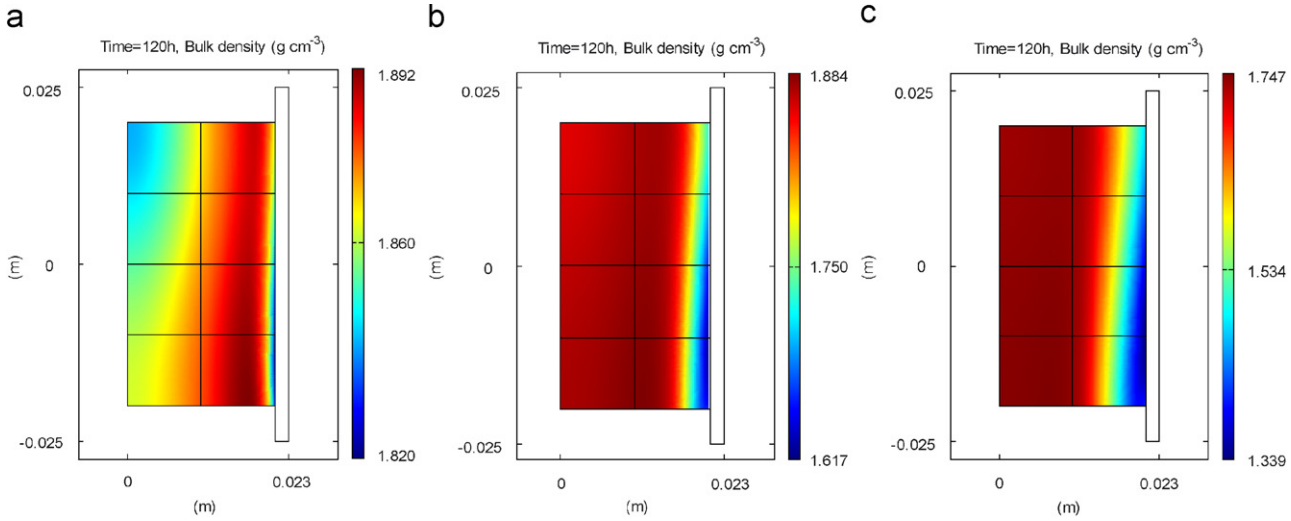

Fig. 5. The predicted bulk density distributions (120 h densification) corresponding to feed gas of (a) 20 kPa CH_4, (b) 20 kPa CH_4 with 4 kPa additional H_2 and (c) 20 kPa CH_4 with 10 kPa additional H_2.

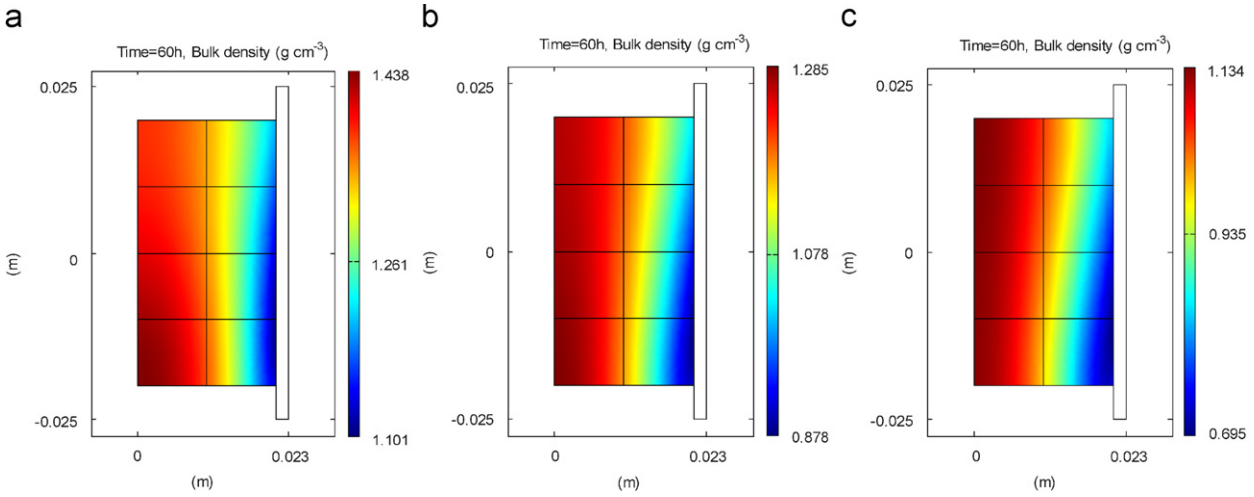

Fig. 6. The predicted bulk density distributions (60 h densification) corresponding to feed gas of (a) 20 kPa CH_4, (b) 20 kPa CH_4 with 4 kPa additional H_2 and (c) 20 kPa CH_4 with 10 kPa additional H_2.

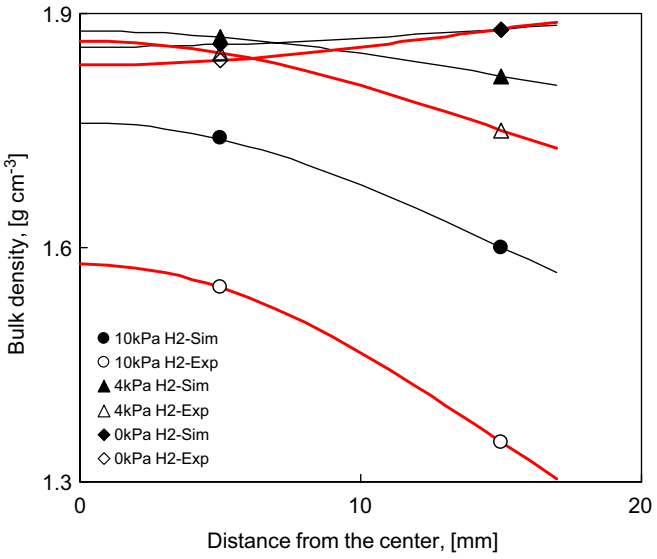

Fig. 7. Bulk density distributions after 120 h densification.

present work, an average density of pyrocarbon is used for the simulation, which cannot distinguish pyrocarbons of different textures. This fact may explain the overprediction of the bulk density for the case of additional 10 kPa H_2.

The surface reaction rates of acetylene formed as an intermediate inside the carbon felt are shown in Figs. 8(a) and (b), for the cases of pure methane and of methane with 4 kPa additional hydrogen, respectively. As a comparison, the reaction rate of benzene corresponding to the case of 10 kPa additional hydrogen is presented in Fig. 8(c). It is clear that the rates of pyrocarbon deposition from the main hydrocarbons in CVI are smaller than those in CVD, because hydrogen inhibition plays a more important role in CVI than in CVD. This suggests the hydrogen inhibition model must be included in the numerical simulation of CVI processes.

Pierson and Lieberman (1975), established a CVD model for carbon deposition which relates gas-phase conditions to the resultant microstructure of deposit at first. They correlated pyrocarbon textures to the $[C_2H_n]/[C_6H_m]$ ratio which

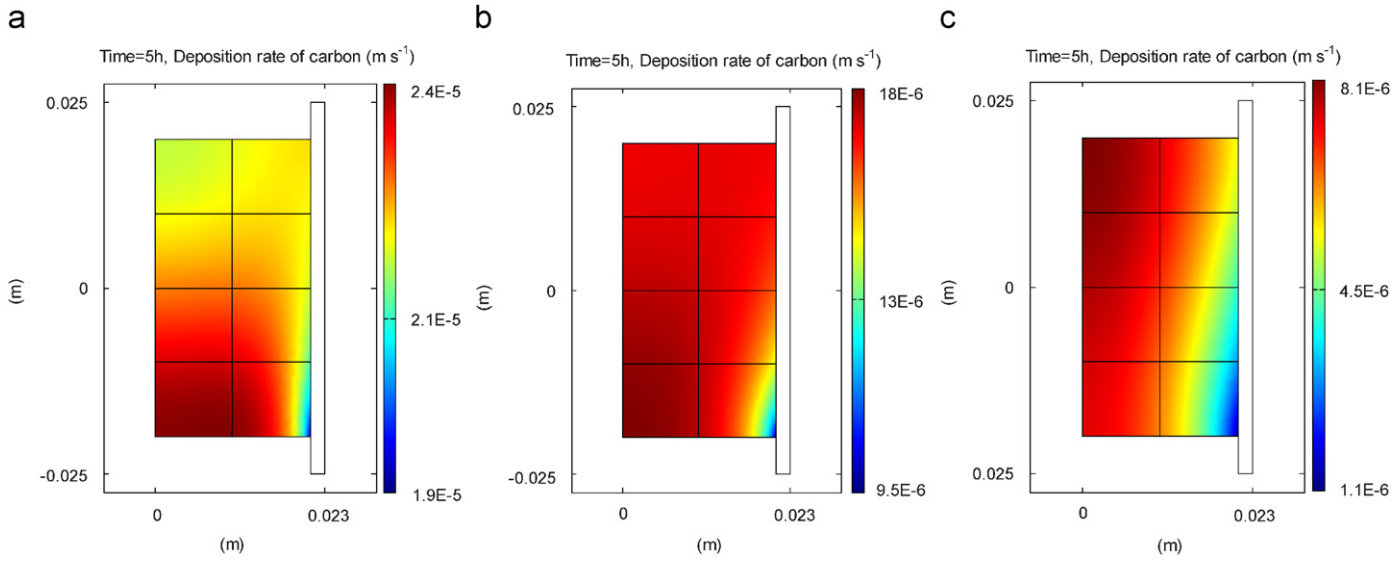

Fig. 8. The local deposition rate of carbon from (a, b) acetylene and (c) benzene, corresponding to feed gas of (a) pure methane, (b) CH_4 with 4 kPa additional H_2 and (c) CH_4 with 10 kPa additional H_2.

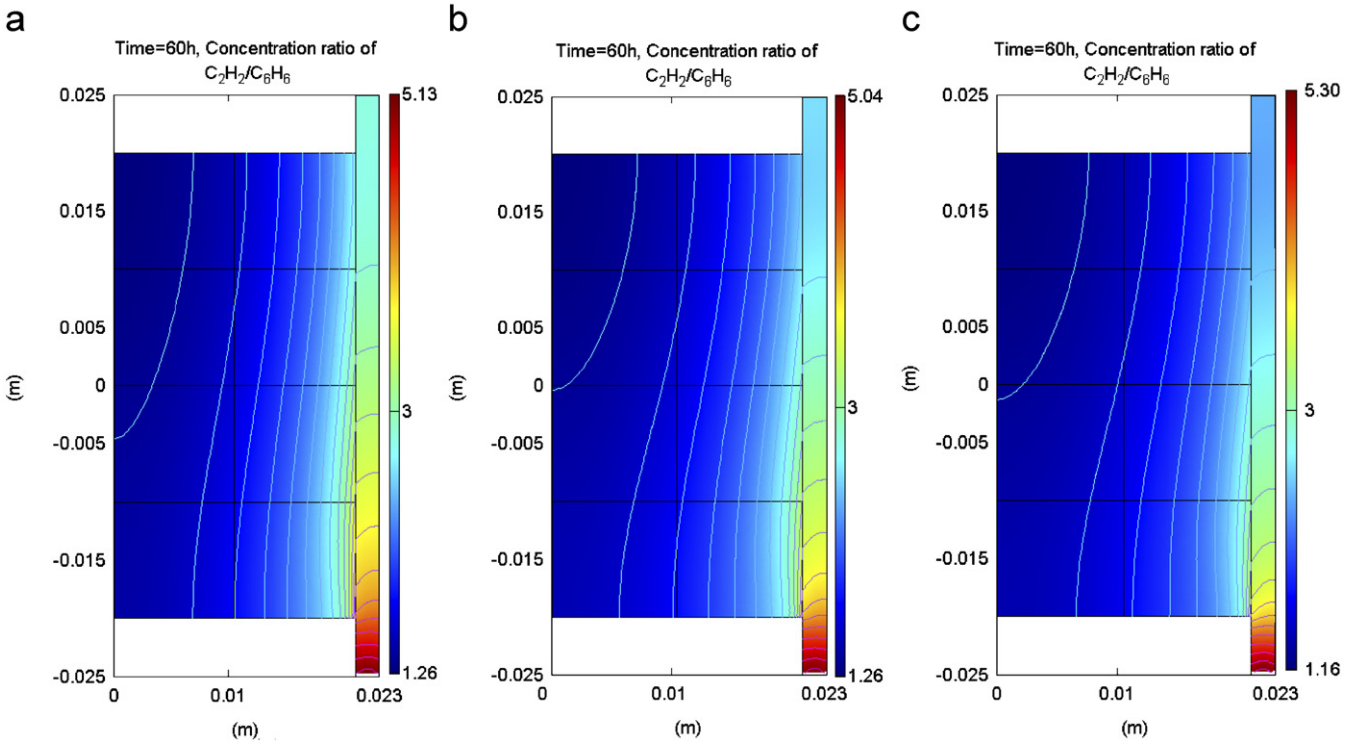

Fig. 9. The concentration ratio of acetylene to benzene corresponding to feed gas of (a) pure methane, (b) CH_4 with 4 kPa additional H_2 and (c) CH_4 with 10 kPa additional H_2.

also means the density of the resultant pyrocarbon depends on the $[C_2H_n]/[C_6H_m]$ ratio in the gas phase. Fig. 9 shows the predicted concentration ratio of acetylene to benzene corresponding to 60 h of densification. In the Figs. 9(a) to (c) one can recognize that, the $[C_2H_n]/[C_6H_m]$ ratio distributions are similar, the bulk density distributions, however, are considerably different as shown in Fig. 6. The clear difference between the simulation and the experimental data for 10 kPa additional hydrogen also suggests that pyrocarbon textures in CVI depend on not only the $[C_2H_n]/[C_6H_m]$ ratio but also on the $[H_2]/[C_xH_y]$ ratio because the consumption of light species differs drastically from that of aromatic species attributed to the stronger hydrogen inhibition of carbon deposition from aromatic species.

4. Summary and outlook

The values of carbon deposition rates measured by CVD experiments can be used for analysis and simulation of CVI

processes if the hydrogen inhibition effect on carbon deposition is taken into account. Bulk density distributions and varying pyrocarbon textures are attributed to both $[H_2]/[C_xH_y]$ and $[C_2H_n]/[C_6H_m]$ ratios. Additional hydrogen may be used to achieve a more uniform density distribution from the bottom to the top of the felts.

To acquire accurate hydrogen inhibition coefficients, systemic CVD experiments will be done at a temperature region from 1273 to 1373 K. Moreover, a new gas-phase reaction mechanism involved in CVI of carbon is being developed on the basis of both experiments and the current pyrolysis mechanism of light hydrocarbons (Norinaga, 2006a, b).

Acknowledgments

We thank Prof. Hüttinger and Prof. Zhang for their suggestions on the hydrogen inhibition model, Dr. Pfrang and Prof. Schimmel for their simulation results of the porosity model, and Dr. Schoch for fruitful discussions on the manuscript. This research was performed in SFB551 (the Sonderforschungsbereich 551) "Carbon from the gas phase: elementary reactions, structures, materials". Financial support by the Deutsche Forschungsgemeinschaft is gratefully acknowledged.

References

Becker, A., Hüttinger, K.J., 1998a. Chemistry and kinetics of chemical vapor deposition of pyrocarbon—II pyrocarbon deposition from ethylene, acetylene and 1,3-butadiene in the low temperature regime. Carbon 36 (3), 177–199.

Becker, A., Hüttinger, K.J., 1998b. Chemistry and kinetics of chemical vapor deposition of pyrocarbon—III pyrocarbon deposition from propylene and benzene in the low temperature regime. Carbon 36 (3), 201–211.

Becker, A., Hu, Z.J., Hüttinger, K.J., 2000. A hydrogen inhibition model of deposition from hydrocarbon. Fuel 79, 1573–1580.

Besmann, T.M., Sheldon, B.W., Lowden, R.A., Stinton, D.P., 1991. Vapor-phase fabrication and properties of continuous-filament ceramic composites. Science 253, 1104–1109.

Benzinger, W., Hüttinger, K.J., 1998. Chemical vapor infiltration of pyrocarbon-II. The influence of increasing methane partial pressure at constant total pressure on infiltration rate and degree of pore filling. Carbon 36 (7–8), 1033–1042.

Birakayala, N., Evans, E.A., 2002. A reduced reaction model for carbon CVD/CVI processes. Carbon 40, 675–683.

Brüggert, M., Hu, Z.J., Hüttinger, K.J., 1999. Chemistry and kinetics of chemical vapor deposition of pyrocarbon VI. Influence of temperature using methane as a carbon source. Carbon 37, 2021–2030.

Delhaès, P., 2002. Chemical vapor deposition and infiltration processes of carbon materials. Carbon 40, 641–657.

Fitzer, E., 1987. The future of carbon/carbon composites. Carbon 25, 163–190.

Hu, Z.J., Hüttinger, K.J., 2001. Chemical vapor infiltration of carbon—revised. Part II: experimental results. Carbon 39, 1023–1032.

Hüttinger, K.J., 1998. CVD in hot wall reactors—the interaction between homogeneous gas-phase and heterogeneous surface reactions. Advanced Materials CVD 4, 151–158.

Li, H.J., Li, A.J., Bai, R.C., Li, K.Z., 2005. Numerical simulation of chemical vapor infiltration of propylene into C/C composites with reduced multistep kinetic models. Carbon 43, 2937–2950.

Norinaga, K., Deutschmann, O., Hüttinger, K.J., 2006a. Analysis of gas phase compounds in chemical vapor deposition of carbon from light hydrocarbons. Carbon 44 (9), 1790–1800.

Norinaga, K., Li, A., Deutschmann, O., 2006b. Detailed kinetic modeling of gas phase reactions in chemical vapor deposition of carbon from light hydrocarbon. Paper presented at the International Carbon Conference, Aberdeen.

Pierson, H.O., Lieberman, M.L., 1975. The chemical vapor deposition of carbon on carbon fibers. Carbon 13, 159–166.

Sheldon, B.W., Besmann, T.M., 1991. Reaction and diffusion kinetics during the initial stages of isothermal chemical vapour infiltration. Journal of the American Ceramic Society 74 (12), 3046–3053.

Starr, T.L., 1988. Deposition kinetics in forced flow/thermal gradient CVI. Ceramic Engineering and Science Proceedings 9 (7–8), 803–811.

Tai, N.H., Chou, T.W., 1989. Analysis modeling of chemical vapor infiltration in fabrication of ceramic composites. Journal of the American Ceramic Society 72 (3), 414–420.

Vignoles, G.L., Goyhénèche, J.-M., Sébastian, P., Puiggali, J.-R., Lines, J.-F., Lachaud, J., Delhaès, P., Trinquecoste, M., 2006. The filmboiling densification process for C/C composite fabrication: from local scale to overall optimization. Chemical Engineering Science 61, 5336–5353.

Zhang, W.G., Hüttinger, K.J., 2002. Chemical vapor infiltration of carbon fiber felt: optimization of densification and carbon microstructure. Carbon 40 (14), 2529–2545.